7

MULTILAYERED QDSSCs WITH PASSIVATION OF Zn CHALCOGENIDE LAYER

7.1 Introduction

In order to achieve high solar cell performance, back electron transfer or recombination at TiO_2/QD/electrolyte interface needs to be minimized [1,2]. This can be achieved by altering the surface chemistry of the TiO_2/QD surface. To date, the most popular method is the deposition of a passivation layer on the TiO_2/QD surface. ZnS has been proven to be a good passivation layer for minimizing recombination process at the TiO_2/QD/electrolyte interface [3]. Besides ZnS, other organic or inorganic materials can also be applied as a passivation layer although some of the results might not be comparable to that obtained from using ZnS [4]. In this study, QDSSCs with TiO_2 co-sensitized with CdS and CdSe were optimized and Zn chalcogenide (ZnS, ZnSe or ZnTe) was used as the passivation layer. The effect of ZnS was first studied. This was followed by assessment on the suitability of other Zn chalcolgenide materials (ZnSe and

ZnTe) as the passivation layer instead of ZnS. To the author's best knowledge, there is no report in the literature on the performance of ZnSe and ZnTe as the passivation layer in QDSSCs.

CdS and CdSe QD-sensitized TiO_2 electrodes were prepared as described in Chapter 3. SILAR parameters for CdS and CdSe QD were set in accordance with the optimization result as reported in Chapter 4. For the deposition of Zn chalcogenide layer, the SILAR dipping was performed as per procedure detailed in section 3.2.3, Chapter 3. The QDs prepared are referred to as CdS(*n*), CdSe(*n*) and ZnX(*n*) respectively, where *n* is the number of SILAR cycles used for preparing them and X = S, Se or Te. Polysulfide electrolyte was prepared based on the optimized result as in Chapter 5. UV-Vis was performed on the electrode samples followed by solar cell performance and EIS study.

7.2 Results and discussion

7.2.1 Surface morphology

SILAR has been used to prepare QDs for sensitization on TiO_2 due to its simplicity and easy control of the QD size [5,6]. Mixed QDs were prepared by depositing CdS QDs first followed by CdSe deposition. The passivation layers were then deposited on top of the QD layers. As the SILAR cycles increased, the colour intensity on the QD-sensitized TiO_2 layer increased as shown in Figure 7.1.

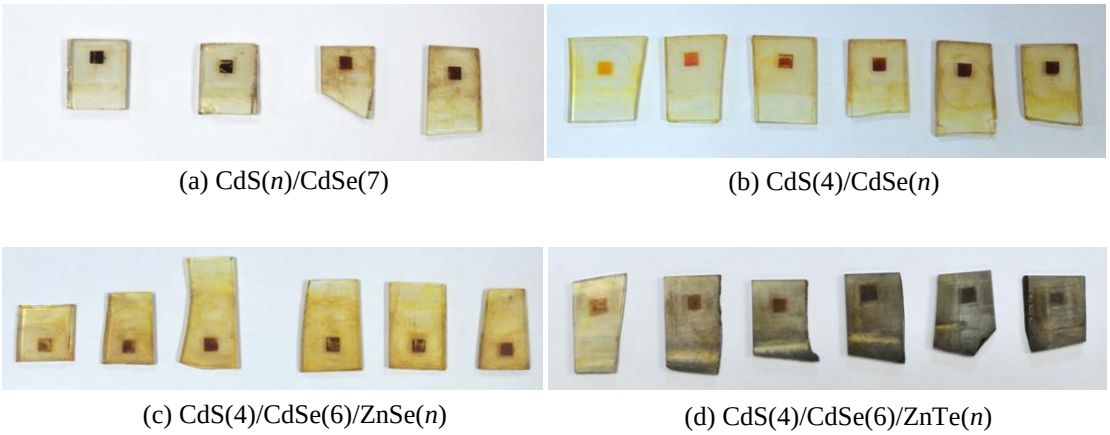

(a) CdS(*n*)/CdSe(7) (b) CdS(4)/CdSe(*n*)

(c) CdS(4)/CdSe(6)/ZnSe(*n*) (d) CdS(4)/CdSe(6)/ZnTe(*n*)

Figure 7.1. The effect of the number of SILAR cycles on the colour change of the QD-sensitized TiO_2 layer. *n* is the number of SILAR cycles which increases sequentially from the most left sample to the right sample.

In Figure 7.1(a), when the number of CdSe QD depositions was fixed at 7 SILAR cycles, and the number of CdS depositions were changed from 1 to 4 cycles, there is only a slight colour change observed. This is due to the significantly strong dark colour of CdSe(7) layer although there was a gradual increase from light yellow to orange corresponding to CdS(1) to CdS(4). However, when the CdS layer was fixed at 4 SILAR cycles and CdSe layer was varied from 1 to 7 SILAR cycles, the change of colour of the QD-sensitized TiO_2 was clearly seen as in Figure 7.1(b). The colour changed from light orange to dark brown. For the CdS(4)/CdSe(7)/ZnSe(*n*) QDs-sensitized TiO_2, the colour change was not significant compared with that of the CdS(4)/CdSe(7)/ZnTe(*n*) QDs-sensitized TiO_2 as shown in Figure 7.1(c) and 7.1(d). It was observed that addition of ZnTe layer had more darkening effect compared with that produced by ZnSe layer which only manifested in dark red. The change of the color with different SILAR cycles is due to the quantum confinement effect of the QDs which corresponds to the change of the QD size [7,8]. As the number of SILAR cycles increased, the QD size usually increased until an optimum size is reached and then decreased due to QDs overcrowding effect.

Observation on surface morphology through FESEM revealed particle size increased with more deposition of QDs. With the sensitization of TiO_2 layer by CdS and CdSe QDs, the particle size appears slightly larger compared with bare TiO_2 layer (see Figure 7.2(a) and (b)). Addition of ZnSe and ZnTe layers seem to form a matrix layer on top of the TiO_2/QD particles (Figure 7.2(c) and (d)). The ZnSe and ZnTe layers look like a barrier which may hinder the electron transfer through the TiO_2 layer (this effect shall be explained in the following sections).

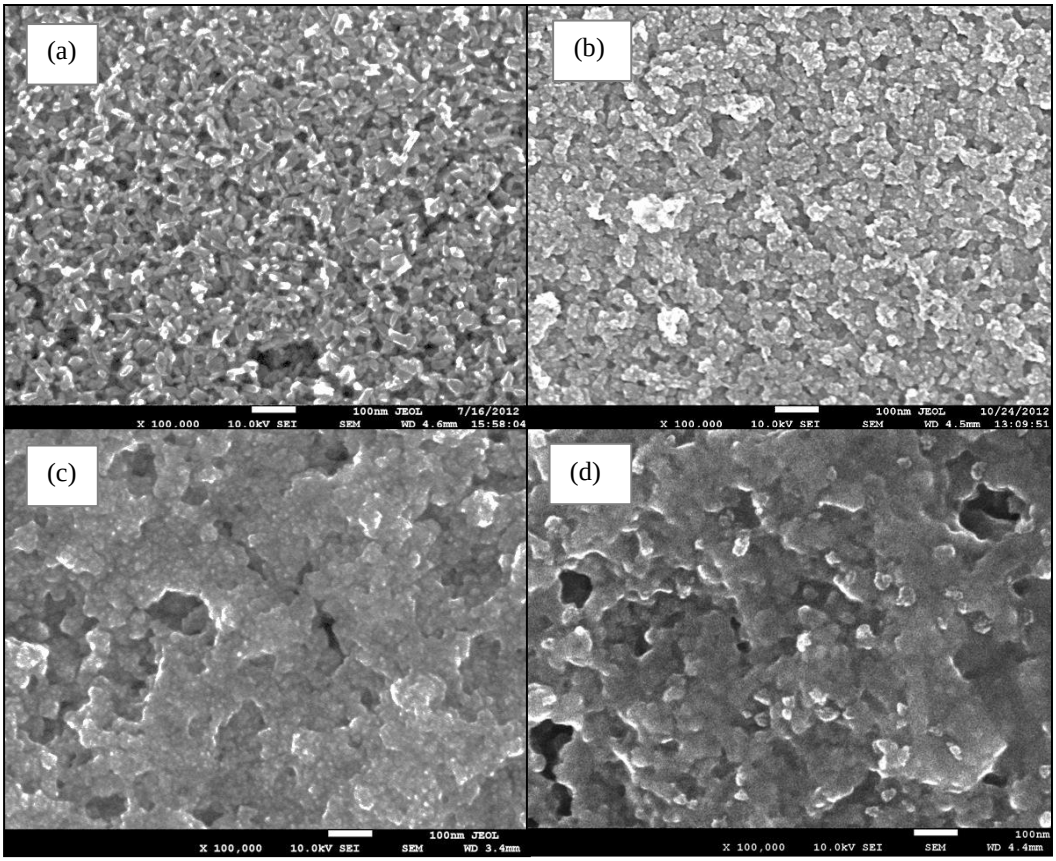

Figure 7.2. FESEM images of (a) bare TiO_2; (b) CdS(4)/CdSe(6) - sensitized TiO_2; (c) CdS(4)/CdSe(6)/ZnSe(6) – sensitized TiO_2; (d) CdS(4)/CdSe(6)/ZnTe(6) – sensitized TiO_2. All images are under 100,000x magnification.

To verify that ZnSe and ZnTe layers had indeed formed on top of CdS/CdSe QDs layers, samples were analyzed via TEM imaging and EDX. TEM images are shown in Figure 7.3 while EDX result is shown in Figure 7.4. It was observed that CdS QDs formed as the underlayer on the TiO_2 particles. This is followed by CdSe QDs forming on top of CdS QDs. The CdS and CdSe QD particles have d-spacing of 0.205 nm and 0.32 nm respectively, as matched with JCPDS library data. Lastly, both ZnSe and ZnTe layers appear as thin layer on top of CdS or CdSe QDs. Their d-spacing values are 0.33 nm and 0.35 nm respectively. The absence of ZnTe on the bare TiO_2 particles suggests that ZnTe passivation layer may require a QD underlayer for seed growth or the growth on TiO_2 particle maybe specific on certain crystallographic planes. Furthermore, ZnTe layer may not be stable and easily degraded upon exposure as in the case of CdTe [9]. Nevertheless, EDX result (Figure 7.4) indicates that Te element is still present in the sample.

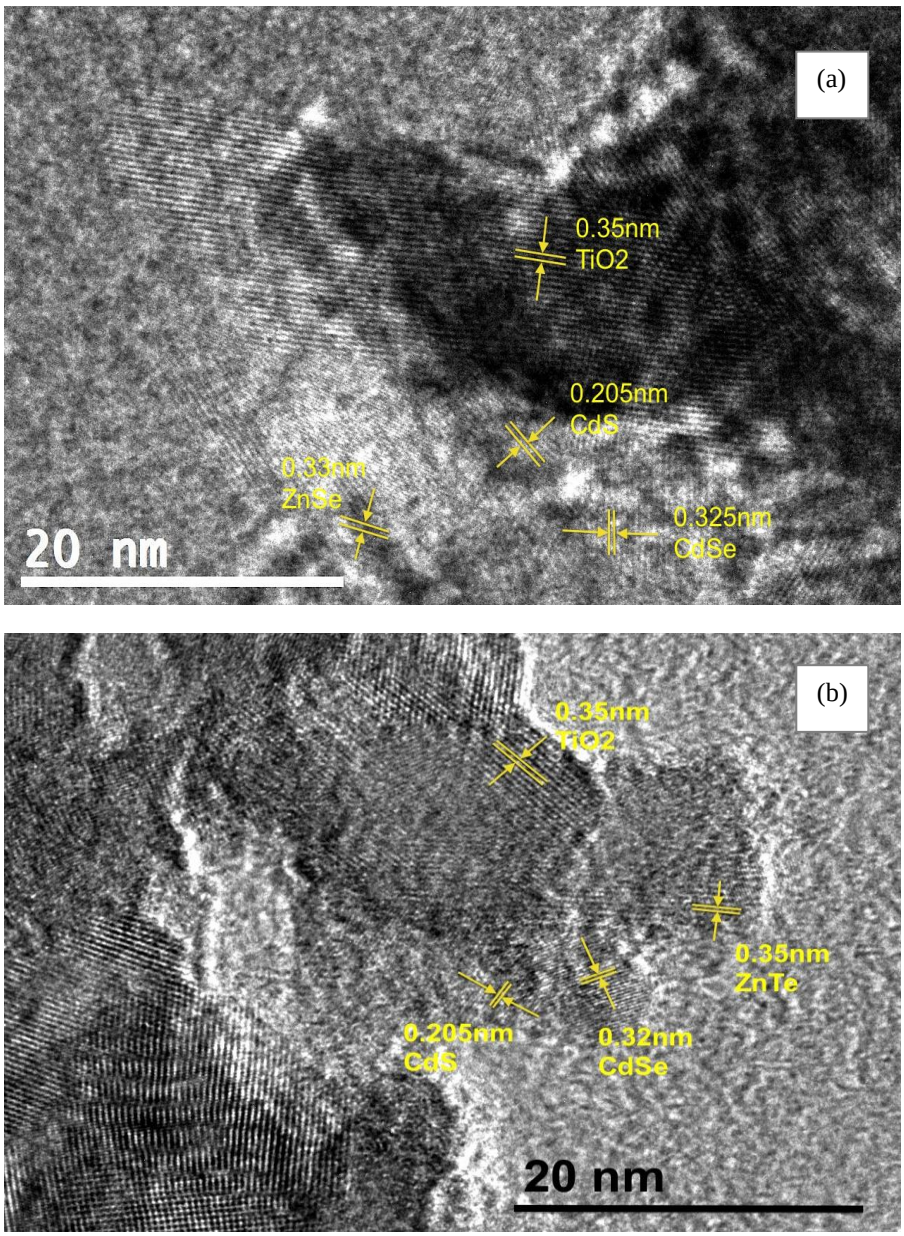

Figure 7.3. TEM images of (a) CdS(4)/CdSe(6)/ZnSe(6) – sensitized TiO_2; (b) CdS(4)/CdSe(6)/ZnTe(6) – sensitized TiO_2.

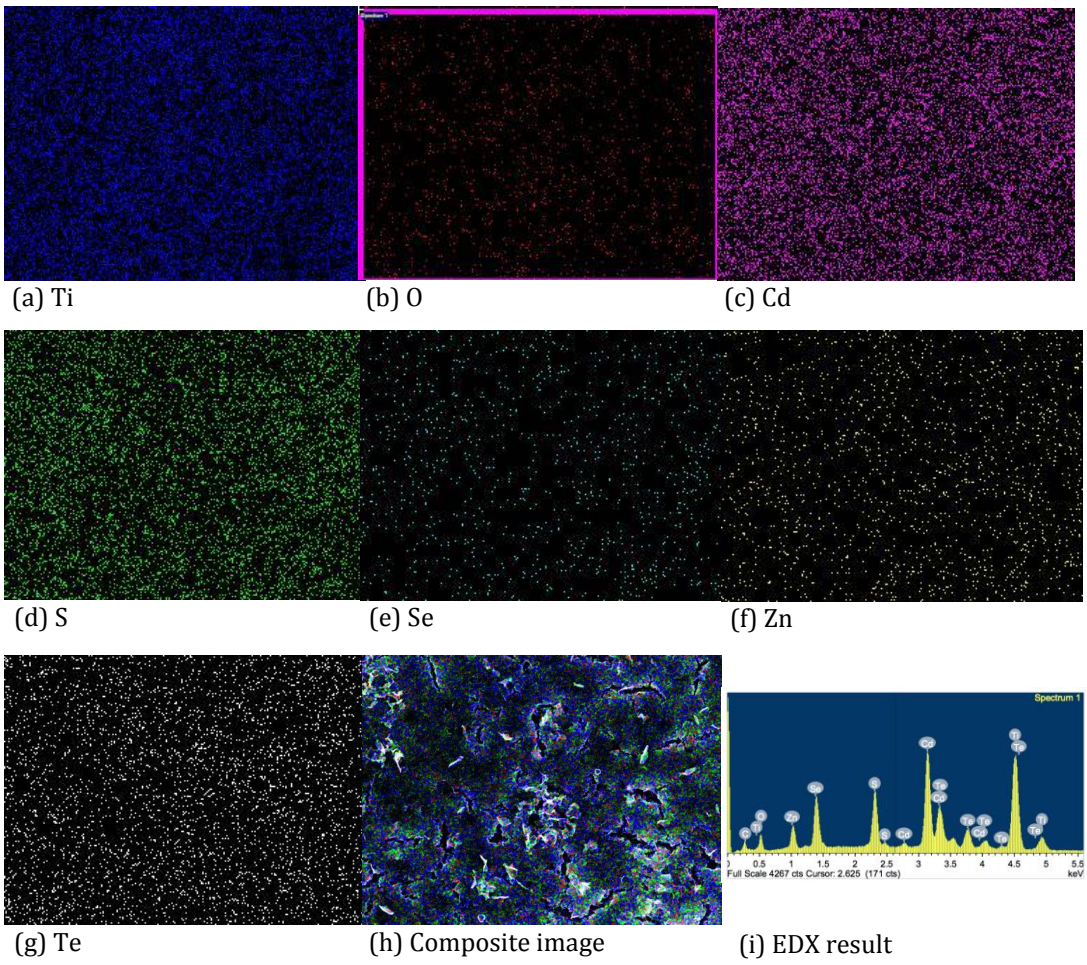

Figure 7.4. EDX mapping analysis of CdS(4)/CdSe(6)/ZnTe(6) – sensitized TiO_2 sample.

7.2.2 *J-V* curves

The performance of the solar cell samples were measured under illumination. The first batch of samples were from CdS(*n*)/CdSe(7) QDSSCs. The SILAR cycle for CdSe layer was set at 7 based on the optimum performance in a separate study. UV-vis spectroscopy results on this batch of sample as shown in Figure 7.5 indicate the absorption edges of the 4 samples do not differ much, which is at around 650 nm. Therefore, it is expected that the solar cell performance may not vary much. However, actual cells performances do not adhere with the UV-vis spectra result (see Figure 7.6 and Table 7.1). CdS(4)/CdSe(7) QDSSC has the best performance with efficiency of 0.91% and photocurrent density of 5.49 mA/cm^2. The worst performance is shown by

the CdS(1)/CdSe(7) QDSSC with an efficiency of 0.51% and low photocurrent density of 2.89 mA/cm^2. It can be concluded that addition of CdS QD underlayer helps to enhance the solar cell performance. However, in this study, the SILAR cycle of CdS deposition was limited to 4 considering the optimum performance was obtained with CdS(4) QDSSC.

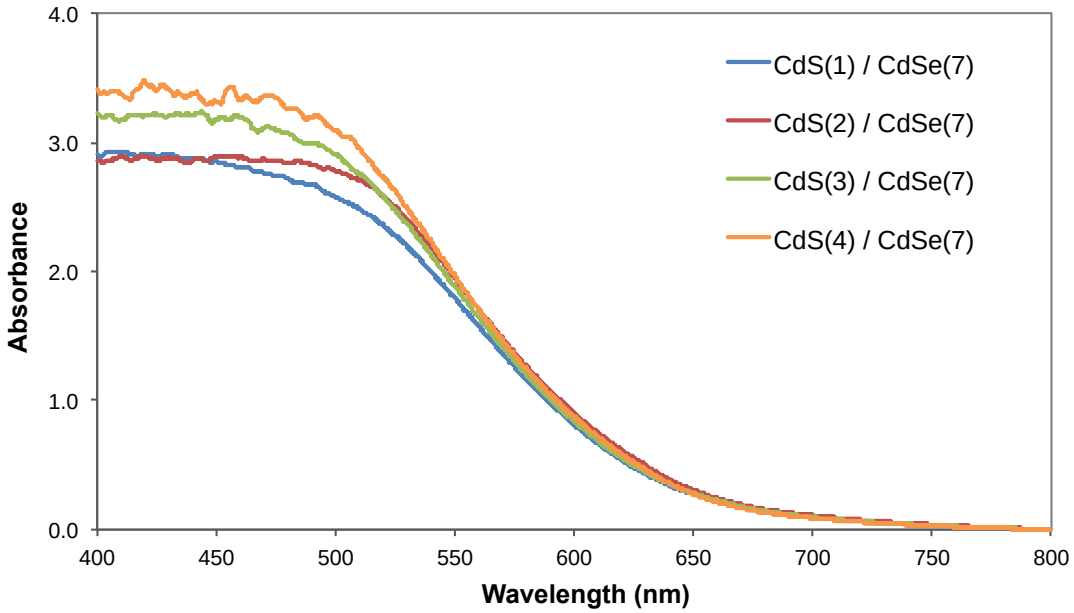

Figure 7.5. UV-vis spectra for CdS(*n*)/CdSe(7)-sensitized TiO_2 where *n* is from 1-4.

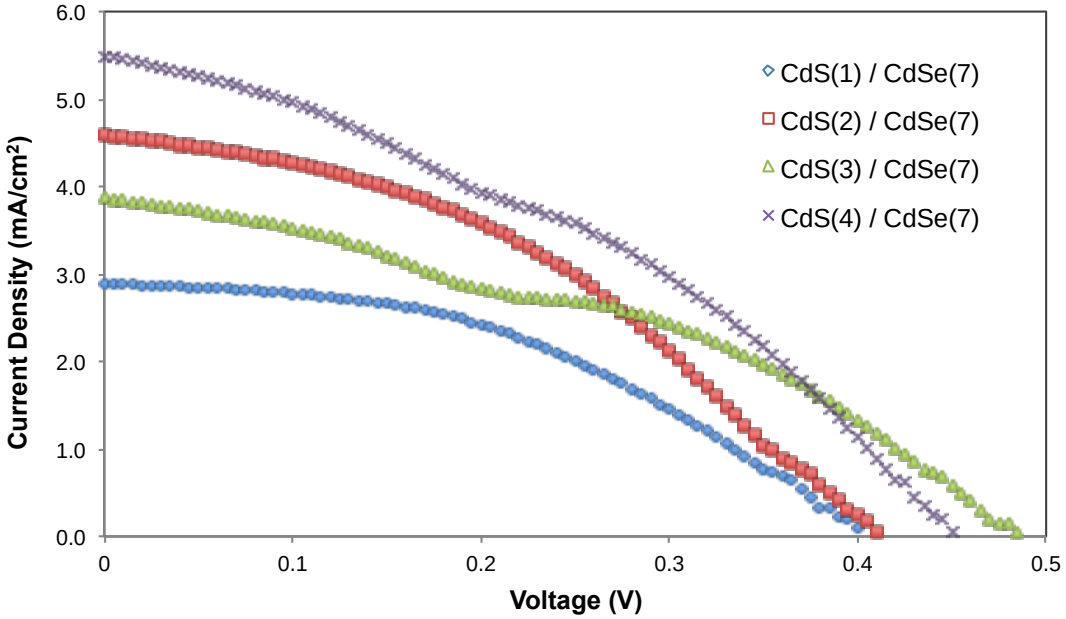

Figure 7.6. *J-V* curves of CdS(*n*)/CdSe(7) QDSSCs.

Table 7.1. Performance parameters of CdS(*n*)/CdSe(7) QDSSCs.

	Jsc (mA/cm^2)	V_{OC} (V)	FF (%)	η (%)
CdS(1) / CdSe(7)	2.89	0.400	44	0.51
CdS(2) / CdSe(7)	4.59	0.410	40	0.75
CdS(3) / CdSe(7)	3.87	0.485	39	0.73
CdS(4) / CdSe(7)	5.49	0.450	37	0.91

With the best solar cell performance obtained in CdS(4)/CdSe(7) QDSSC, now the optimum SILAR cycle for CdSe QD deposition needs to be determined when the CdS QD underlayer is deposited with 4 SILAR cycles. As the CdSe QD deposition increased, the absorbance intensity of the QD-sensitized TiO_2 film also increased as seen in Figure 7.7. However, the absorption edges of the cells only change slightly, within the range of 625 – 675 nm. With increasing SILAR cycles of CdSe QD deposition, there is a reduction of effective band gap energy which suggests a red-shift effect. For low band energy, the estimated effective QD diameter will be large as in the case of CdS(4)/CdSe(6)-sensitized TiO_2 film. The shifting of the absorption edge with the number of SILAR cycles for CdSe deposition indicates the tunability of the effective band gap energy of the QDs.

In terms of cell performance, CdS(4)/CdSe(6) QDSSC gives the highest efficiency among the samples as shown in Figure 7.8 and Table 7.2. It recorded an efficiency of 1.12% with photocurrent density of 5.85 mA/cm^2. This efficiency is higher than that of the previous cell in CdS(*n*)/CdSe(7) QDSSC batch and is slightly better than the reported result of 1.06% [10]. However, it is also lower than other reported result which is above 1.50% [11,12]. This difference could be attributed to the growth of QDs during the SILAR process as a longer time for rinsing and drying is beneficial for QDs growth. As a result, distribution of QDs could be inhomogeneous within the TiO_2 layer [13]. Nevertheless, with the increase of SILAR cycles number for the deposition of CdSe QD, the efficiency of the cell increased gradually until a maximum value is reached for CdS(4)/CdSe(6) QDSSC. The better photocurrent injection in that cell is attributed to the well alignment of the energy band positions of the CdS(4)/CdSe(6) cascade structure [14,15]. However, as more CdSe QD layers were deposited, the performance started to deteriorate due to overcrowding of QDs which may slow down the charge transfer from the QDs to the TiO_2 and substrate. The same effect was also observed in Zhang *et al.*'s work in which more QDs deposition led to a detrimental effect on the generation and collection of the charge carriers [11]. In Figure 7.8 and Table 7.2, the *J-V* characteristic and the corresponding performance parameters of the cell made with CdSe(7) are also shown. The performance of CdSe(7) QDSSC does not differ much with CdS(4)/CdSe(7) QDSSC which indicates the redundancy of CdS underlayer in the multilayered structure [16]. Nevertheless, this only applies when the CdSe is deposited in more than six SILAR cycles, as in this study the performance of CdSe(6) QDSSC (refer to result in section 4.2.3.2, Chapter 4) is inferior to those of CdSe(7) QDSSC and CdS(4)/CdSe(6) QDSSC.

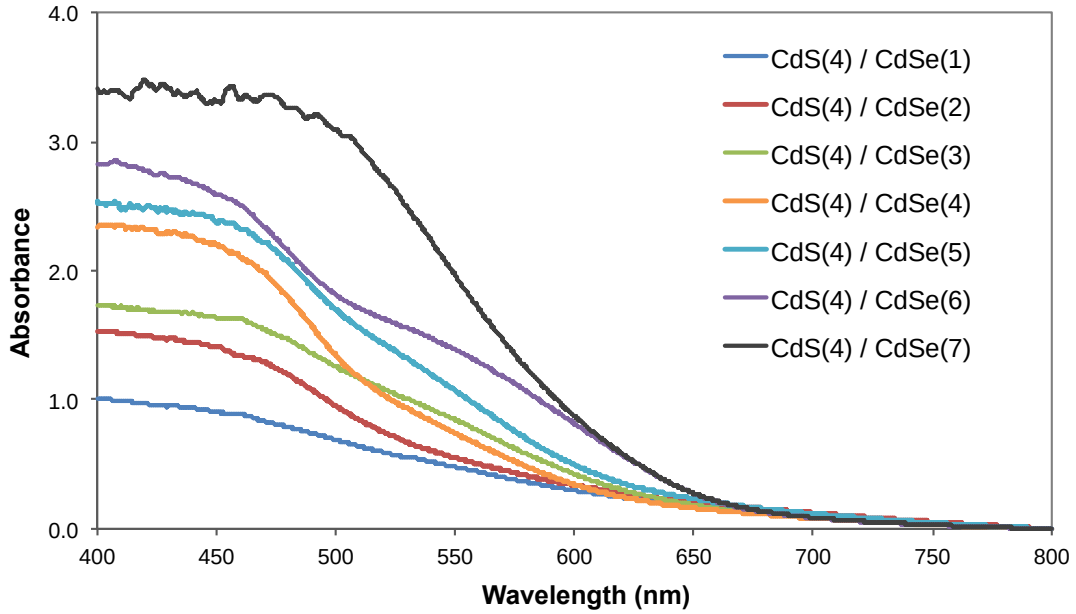

Figure 7.7. UV-vis spectra for CdS(4)/CdSe(*n*)-sensitized TiO_2 where *n* is from 1-7.

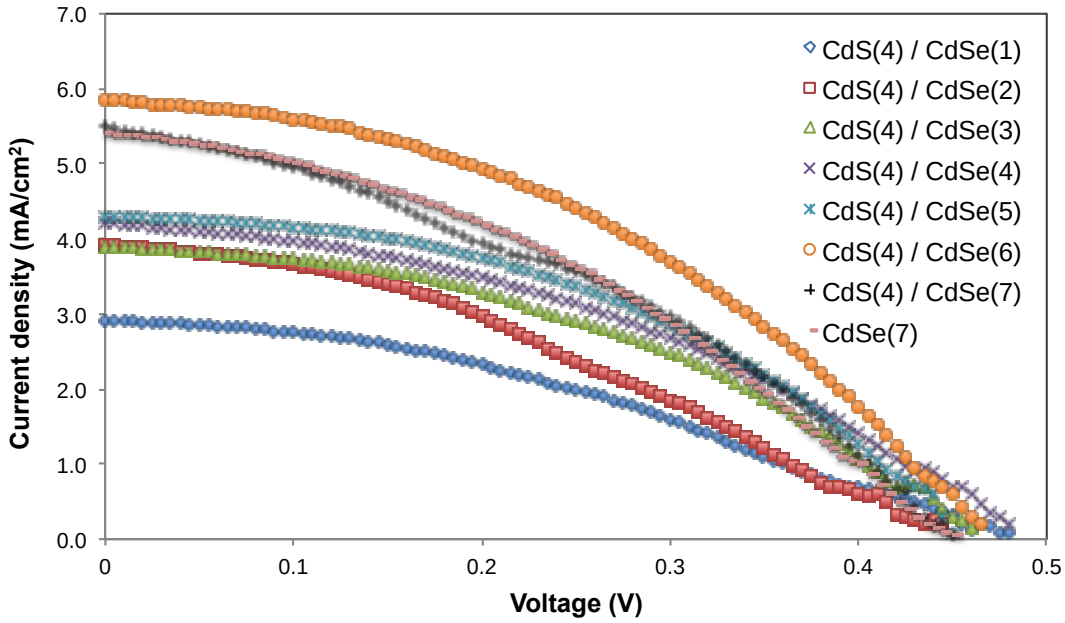

Figure 7.8. *J-V* curves of CdS(4)/CdSe(*n*) QDSSCs.

Table 7.2. Performance parameters of CdS(4)/CdSe(*n*) QDSSCs.

	Jsc (mA/cm^2)	V_{OC} (V)	FF (%)	η (%)
CdS(4) / CdSe(1)	2.92	0.480	36	0.50
CdS(4) / CdSe(2)	3.92	0.450	34	0.60
CdS(4) / CdSe(3)	3.90	0.460	42	0.75
CdS(4) / CdSe(4)	4.20	0.480	40	0.81
CdS(4) / CdSe(5)	4.30	0.450	45	0.87
CdS(4) / CdSe(6)	5.85	0.465	41	1.12
CdS(4) / CdSe(7)	5.49	0.450	37	0.91
CdSe(7)	5.41	0.450	37	0.90

ZnS layer deposited on top of CdS/CdSe layer has proven to bring positive effect on the cell performance similar to the effects as observed in single CdS or CdSe QDSSC [3,12,14,17,18]. In this study, the best performing cell with CdS(4)/CdSe(6) QDs structure was used to study the effect of an additional ZnS layer. The deposition of ZnS was made using two SILAR cycles only based on the literature reports that such ZnS layer gives the best performance [3,12]. As shown in Figure 7.9 and Table 7.3, the addition of ZnS layer has improved the photocurrent density and increased the efficiency by 22%.

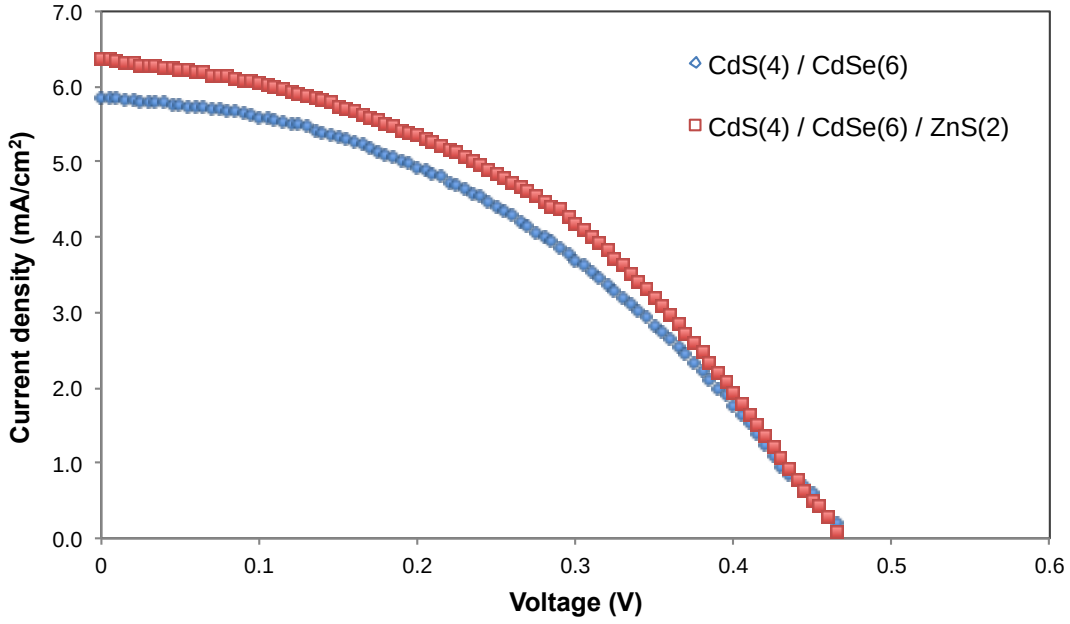

Figure 7.9. *J-V* curves of CdS(4)/CdSe(6) QDSSCs with and without ZnS layer.

Table 7.3. Performance parameters of CdS(4)/CdSe(6) QDSSCs with and without ZnS layer.

	Jsc (mA/cm^2)	V_{OC} (V)	FF (%)	η (%)
CdS(4) / CdSe(6)	5.85	0.465	41	1.12
CdS(4) / CdSe(6) / ZnS(2)	6.37	0.465	45	1.37

On the other hand, if the ZnS layer was substituted with other Zn chalcogenide layer such as ZnSe and ZnTe, it was expected the cell performance should improve as well. In the next study, ZnSe layer was deposited on top of CdS(4)/CdSe(6)-sensitized TiO_2 film using 1 to 6 SILAR cycles. The performances of these solar cells are shown in Figure 7.10 and the performance parameters are tabulated in Table 7.4. With ZnSe as the passivation layer on QD-sensitized TiO_2 film, the cell performance is found to decrease compared to that of the cell having ZnS as passivation layer. The major effect of adding ZnSe is the decrease in open-circuit voltage. However, as the number of ZnSe SILAR cycles deposition increased, the efficiency of the solar cell is increased as well. This effect is largely assigned to the photocurrent density trend. Photocurrent density increased in tandem with more ZnSe SILAR cycles deposition except for CdS(4)/CdSe(6)/ZnSe(2) QDSSC. The slightly higher value of photocurrent density in this solar cell could be attributed to the faster charge injection in QDs owing to better band energy alignment of the cascade CdS(4)/CdSe(6)/ZnSe(2) structure. In general, more ZnSe deposition should contribute to the improvement of charge injection as it has band gap energy of 2.7 eV. The low band gap energy level of ZnSe compared to ZnS implies that ZnSe could take part in the photocurrent transportation instead of functioning as passivation layer. This phenomenon was supported by UV-vis spectroscopy of the batch as shown in Figure 7.11. On the other hand, the overall low open-circuit voltage indicates slow hole reduction from the QD to the electrolyte. Perhaps a better performance can be expected with a better redox mediator. The highest performance is obtained when ZnSe was deposited with 6 SILAR cycles. It is expected that the efficiency could go even higher with a few more SILAR cycles. However, with

more deposition of ZnSe QDs, QD overcrowding may affect the performance of the solar cells.

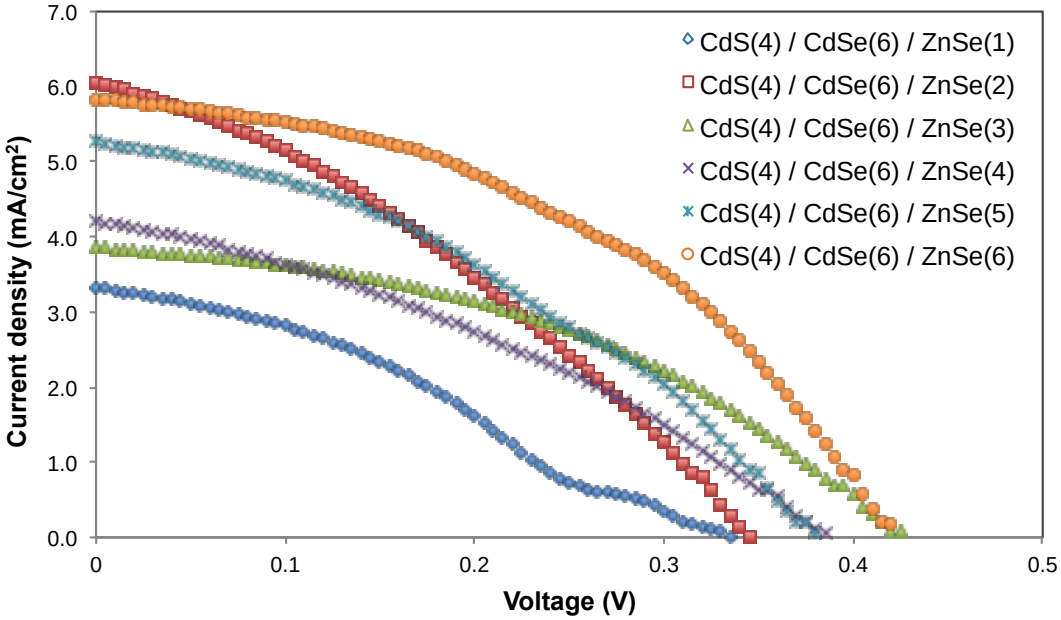

Figure 7.10. *J-V* curves of CdS(4)/CdSe(6)/ZnSe(*n*) QDSSCs.

Table 7.4. Performance parameters of CdS(4)/CdSe(6)/ZnSe(*n*) QDSSCs.

	Jsc (mA/cm^2)	V_{OC} (V)	FF (%)	η (%)
CdS(4) / CdSe(6) / ZnSe(1)	3.32	0.335	32	0.36
CdS(4) / CdSe(6) / ZnSe(2)	6.06	0.345	33	0.69
CdS(4) / CdSe(6) / ZnSe(3)	3.86	0.425	42	0.69
CdS(4) / CdSe(6) / ZnSe(4)	4.21	0.385	34	0.55
CdS(4) / CdSe(6) / ZnSe(5)	5.26	0.380	36	0.72
CdS(4) / CdSe(6) / ZnSe(6)	5.82	0.420	44	1.08

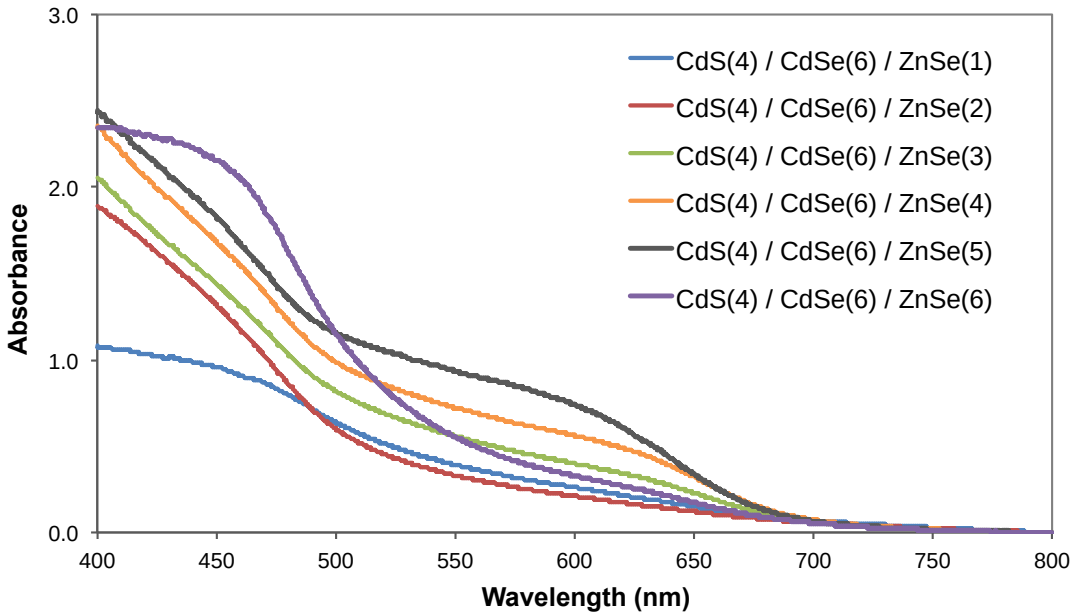

Figure 7.11. UV-vis spectra for CdS(4)/CdSe(6)/ZnSe(*n*)-sensitized TiO_2, where *n* changes from 1-6.

In the following study, ZnTe layer was deposited on CdS(4)/CdSe(6) QD-sensitized TiO_2 film with SILAR cycles ranging from 1 to 6. The *J-V* curves of the cells are shown in Figure 7.12 while Table 7.5 lists the performance parameters of the cells. From the results, it can be seen that the efficiency of the cells decreased with the increasing number of SILAR cycles used for the deposition of ZnTe. The highest performance was obtained in CdS(4)/CdSe(6)/ZnTe(1) QDSSC with an efficiency of 0.90%. This result is similar to that obtained for CdSe(7) QDSSC indicating the redundancy of ZnTe layer. In fact, the deterioration of the cell performance increased with more ZnTe SILAR cycles deposition. The decrease of the photocurrent density with more ZnTe layers shows the negative effect on charge injection with the addition of ZnTe layer. However, the open-circuit voltage of the batch is higher compared with that of the previous batch of CdS(4)/CdSe(6)/ZnSe(*n*) QDSSCs. This result shows that ZnTe may not be suitable to be applied as a passivation layer in QDSSCs. The negative effect of the cells with ZnTe layer could be due to energy band misalignment within the cascade structure of CdS(4)/CdSe(6)/ZnSe(*n*).

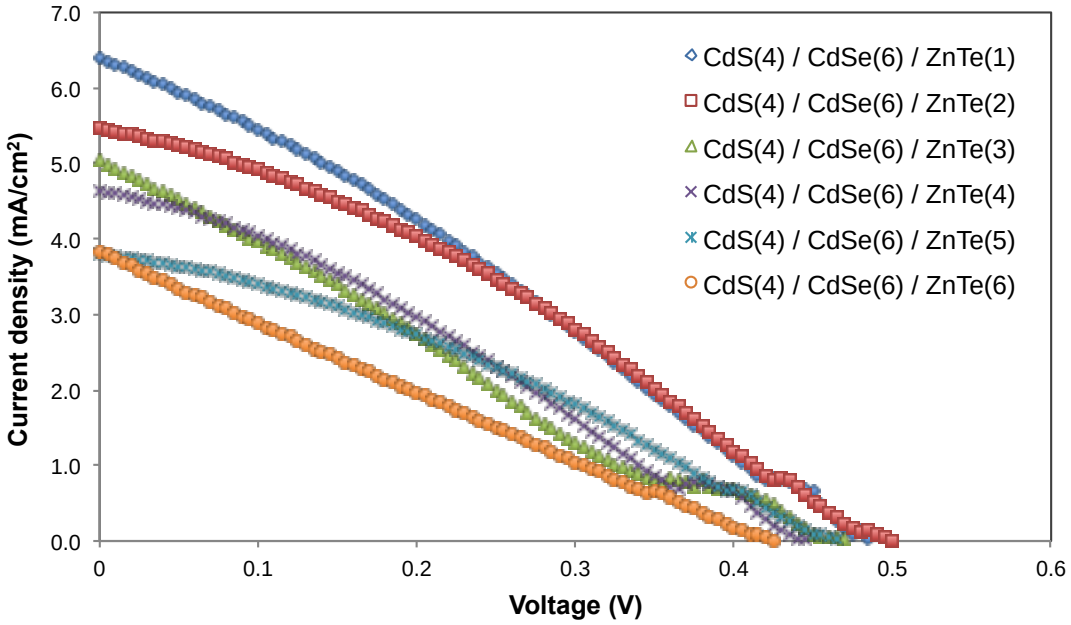

Figure 7.12. *J-V* curves of CdS(4)/CdSe(6)/ZnTe(*n*) QDSSCs.

Table 7.5. Performance parameters of CdS(4)/CdSe(6)/ZnTe(*n*) QDSSCs.

	Jsc (mA/cm^2)	V_{OC} (V)	FF (%)	η (%)
CdS(4) / CdSe(6) / ZnTe(1)	6.39	0.485	29	0.90
CdS(4) / CdSe(6) / ZnTe(2)	5.46	0.500	32	0.87
CdS(4) / CdSe(6) / ZnTe(3)	5.03	0.470	23	0.54
CdS(4) / CdSe(6) / ZnTe(4)	4.64	0.445	29	0.60
CdS(4) / CdSe(6) / ZnTe(5)	3.80	0.465	33	0.58
CdS(4) / CdSe(6) / ZnTe(6)	3.84	0.425	24	0.39

7.2.3 EIS measurements

The behaviour of QDSSC is investigated with EIS analysis. A typical EIS spectrum consists of three semicircles in the Nyquist plot [19,20]. Interpretation of the plot is explained in section 6.2, Chapter 6. Most of the time, only a double arc is observed for a low performance QDSSC in which the feature of electrolyte diffusion is rarely present. In this study, the transmission line model is applied for the curve fitting [21]. The equivalent circuit of QDSSC in a conductive state comprises a combination of

a series resistance and two time constant elements. The time constant element is made up of a resistor in parallel with a constant phase element (CPE). As all the QDSSCs had the same liquid electrolyte and CE material, the resistance and impedance at CE/electrolyte interface should not differ much. The variation in the series resistance could be due to difference in the surface roughness and thickness of the compact layer and CE.

Figure 7.13 shows the Nyquist plots of CdS(*n*)/CdSe(7) QDSSC batch. The corresponding resistance and impedance data are listed in Table 7.6. All the cells in this batch were measured at 0.45 V potential bias under dark condition. The series resistances (R_S) lie between the range of 30 – 40 Ω. If a highly conductive material is used as CE such as Cu_2S, the series resistance is expected to reduce. The charge transfer resistances at photoanode/electrolyte interface (R_r) of the batch do not vary much. However, the true chemical capacitance (C_μ) increases with increasing number of SILAR cycles used for the CdS QD. Consequently, the electron lifetime of the cells is increased with higher number of SILAR cycles of CdS QD which indicates a slower recombination rate of the electron at that interface. This result correlates with the efficiency result obtained from *J-V* curves as in the case of CdS(4)/CdSe(7) QDSSC. The electron lifetime, τ was calculated using equation 7.1 by incorporating the true chemical capacitance value [22].

$$\tau = R_r C_\mu \qquad (7.1)$$

$$= [(\text{CPE-T}) \times R_r]^{1/n} \qquad (7.1a)$$

A higher value of τ is favourable as electron recombination is prolonged at the photoanode/electrolyte interface.

For the batch of CdS(4)/CdSe(*n*) QDSSCs, the Nyquist plots are shown in Figure 7.14 and the EIS data are presented in Table 7.7. The samples were measured at 0.45 V potential bias under dark. Compared with the previous batch of cells, the R_r value appears slightly higher on average. This increase is due to the additional CdSe QDs which can produce additional resistance in the charge transfer pathway. Similarly, the true chemical capacitance is increased with increasing number of SILAR cycles of CdSe QD. However, as the optimum performance is exhibited by the CdS(4)/CdSe(6) QDSSC, the true chemical capacitance value begins to reduce with more CdSe QD layers. The electron lifetime of the samples correlates well with the performance of the solar cell. The longest electron lifetime, 74.87 ms is observed in CdS(4)/CdSe(6) QDSSC for which the efficiency is the highest.

The best performing CdS/CdSe QDSSC with ZnSe and ZnTe as the passivation layer was further analyzed with EIS. For the batch of CdS(4)/CdSe(6)/ZnSe(*n*) QDSSCs, Nyquist plot results are shown in Figure 7.15 and the EIS data are presented in Table 7.8. As more ZnSe layers are added on top of the CdS(4)/CdSe(6) QD structure, the R_r increases, indicating more resistive pathway for the electron to go through. However, the R_r for CdS(4)/CdSe(6)/ZnSe(6) QDSSC is substantially lower compared to the rest in the series. The author does not rule out the possibility of enhanced photocurrent injection in the cell. Although the charge transfer resistance is low, the calculated true chemical capacitance of this cell is high resulting in longer electron lifetime, 19.21 ms. This conforms well with the high efficiency of the cell as explained in the previous section. In general, the electron lifetime of the cell increased with more SILAR cycles used for the ZnSe deposited. This substantiates the author's hypothesis that ZnSe acts as photocurrent transporter rather than as a passivation barrier.

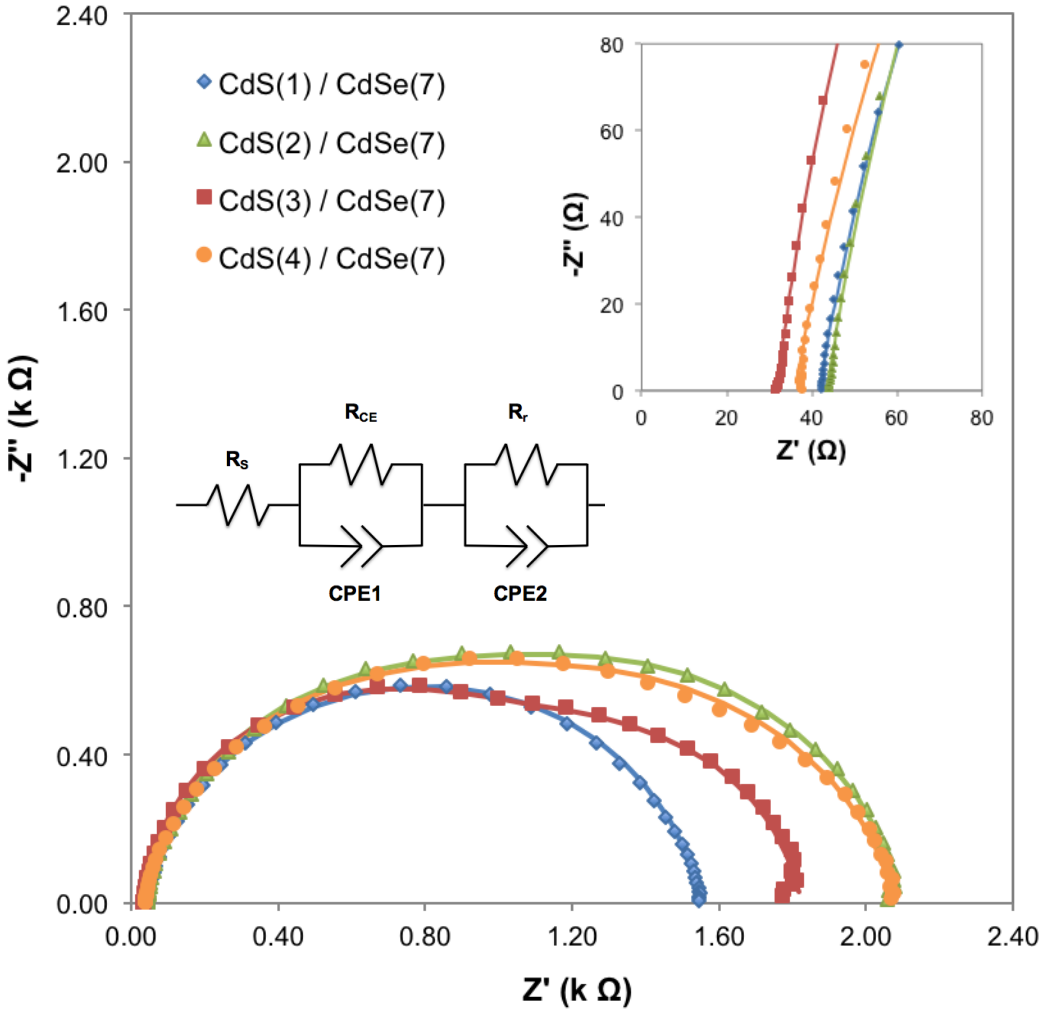

Figure 7.13. Nyquist plots of CdS(*n*)/CdSe(7) QDSSCs under dark with 0.45 V bias. The equivalent circuit of the QDSSC with the representation of series resistance (subscript s), impedance at QD-sensitized TiO_2/electrolyte (subscript r) and counter electrode/electrolyte interface (subscript CE). The symbol R and CPE denote the resistance and constant phase element, respectively. Details of the plots at high-frequencies are showed in the inset. The solid lines are the fitted curves.

Table 7.6. EIS results of CdS(*n*)/CdSe(7) QDSSCs under dark with 0.45 V bias: series resistance, charge-transfer resistance, impedance and electron lifetime.

	R_S (Ω)	R_r (k Ω)	CPE2-T (μ S.s^n)	CPE2-P (0<n<1)	τ (m s)
CdS(1) / CdSe(7)	41.68	0.97	15.90	0.88	8.93
CdS(2) / CdSe(7)	43.61	1.15	31.22	0.87	21.92
CdS(3) / CdSe(7)	31.96	0.82	61.72	0.88	33.63
CdS(4) / CdSe(7)	35.90	0.92	69.66	0.90	46.46

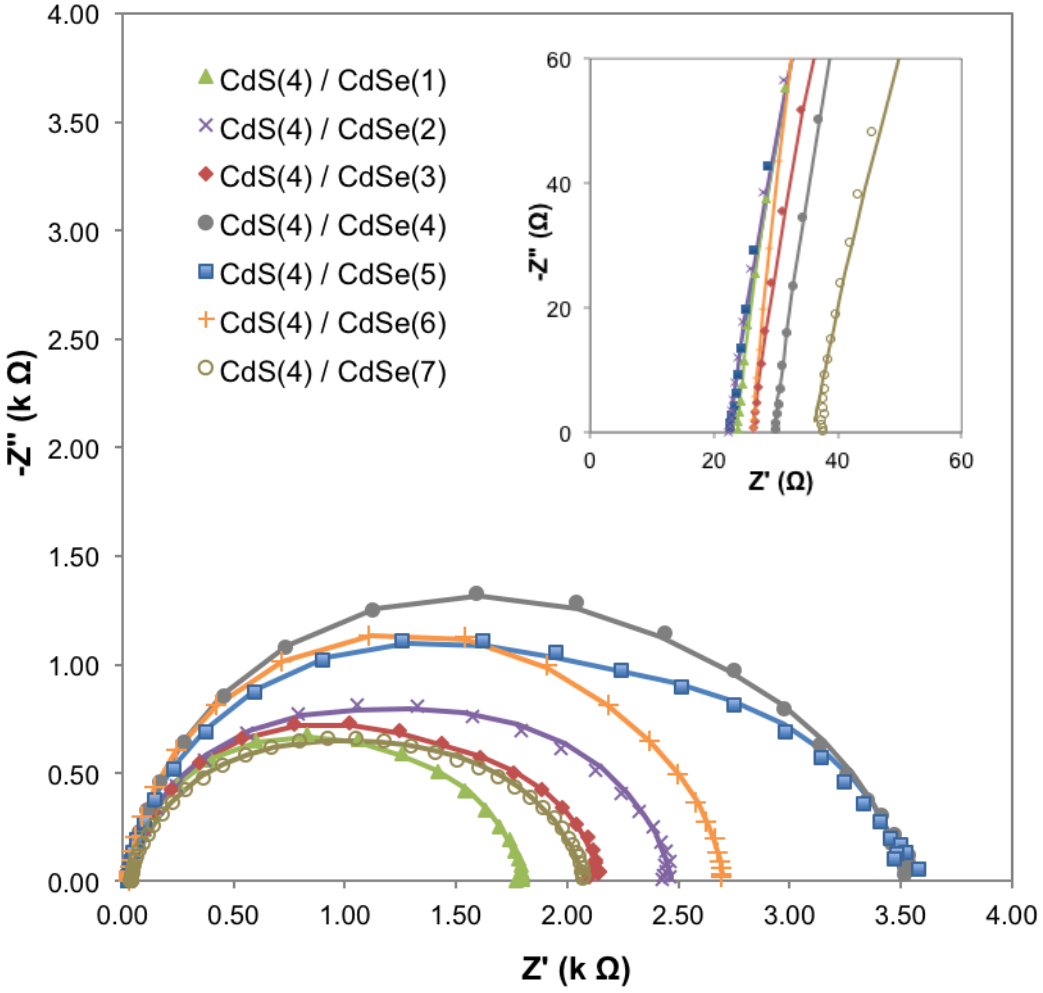

Figure 7.14. Nyquist plots of CdS(4)/CdSe(*n*) QDSSCs under dark with 0.45 V bias. Details of the plots at high-frequencies are shown in the inset. The solid lines are the fitted curves.

Table 7.7. EIS results of CdS(4)/CdSe(*n*) QDSSCs under dark with 0.45 V bias: series resistance, charge-transfer resistance, impedance and electron lifetime.

	R_S (Ω)	R_r (k Ω)	CPE2-T (μ S.s^n)	CPE2-P (0<n<1)	τ (m s)
CdS(4) / CdSe(1)	23.61	1.10	3.72	0.94	2.84
CdS(4) / CdSe(2)	22.20	1.07	6.61	0.93	4.82
CdS(4) / CdSe(3)	26.11	0.82	46.91	0.89	25.44
CdS(4) / CdSe(4)	29.62	1.00	58.17	0.88	38.75
CdS(4) / CdSe(5)	22.27	1.56	65.43	0.84	66.45
CdS(4) / CdSe(6)	26.23	1.27	66.78	0.95	74.87
CdS(4) / CdSe(7)	35.90	0.92	69.66	0.90	46.46

In CdS(4)/CdSe(6)/ZnTe(*n*) QDSSC, the R_r observed is inconsistent with the number of SILAR cycles used for the deposition of ZnTe. The Nyquist plots of the batch are shown in Figure 7.16 while the EIS data is presented in Table 7.9. In most cases, the R_r increased with the addition of ZnTe layers except for the CdS(4)/CdSe(6)/ZnTe(6) QDSSC. This cell has a lower true chemical capacitance as well which yields a low electron lifetime value. As a result, it has the worst performance within the batch. With the increase of ZnTe SILAR cycles, the electron lifetime reduced gradually signifying a faster electron recombination at the photoanode/electrolyte interface. It is perceived that there could be a band energy misalignment in the CdS(4)/CdSe(6)/ZnTe(*n*) cascade structure. As a result, charge transfer is hindered and charge recombination is preferred at the photoanode/electrolyte interface. As there is no significant improvement in electron lifetime, ZnTe is not suitable as a passivation layer or photocurrent transporter.

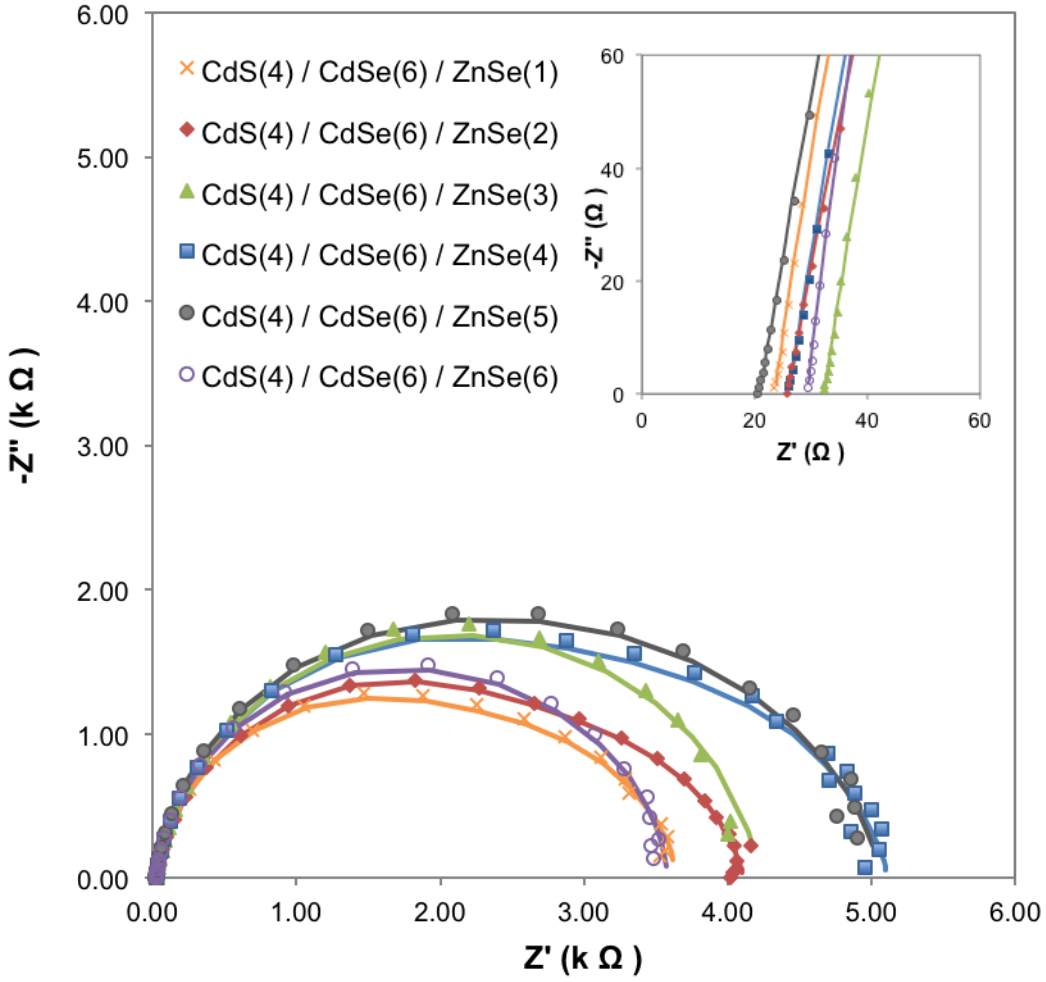

Figure 7.15. Nyquist plots of CdS(4)/CdSe(6)/ZnSe(*n*) QDSSCs under dark with 0.40 V bias. Details of the plots at high-frequencies are shown in the inset. Solid lines are the fitted curves.

Table 7.8. EIS results of CdS(4)/CdSe(6)/ZnSe(*n*) QDSSCs under dark with 0.40 V bias: series resistance, charge-transfer resistance, impedance and electron lifetime.

	R_S (Ω)	R_r (k Ω)	CPE2-T (μ S.s^n)	CPE2-P (0<n<1)	τ (m s)
CdS(4) / CdSe(6) / ZnSe(1)	23.56	2.09	4.87	0.92	6.92
CdS(4) / CdSe(6) / ZnSe(2)	25.86	2.60	5.18	0.90	8.24
CdS(4) / CdSe(6) / ZnSe(3)	32.29	2.76	5.00	0.91	8.81
CdS(4) / CdSe(6) / ZnSe(4)	26.03	2.74	4.15	0.92	7.69
CdS(4) / CdSe(6) / ZnSe(5)	20.74	2.03	6.54	0.95	10.77
CdS(4) / CdSe(6) / ZnSe(6)	29.30	1.10	22.20	0.94	19.21

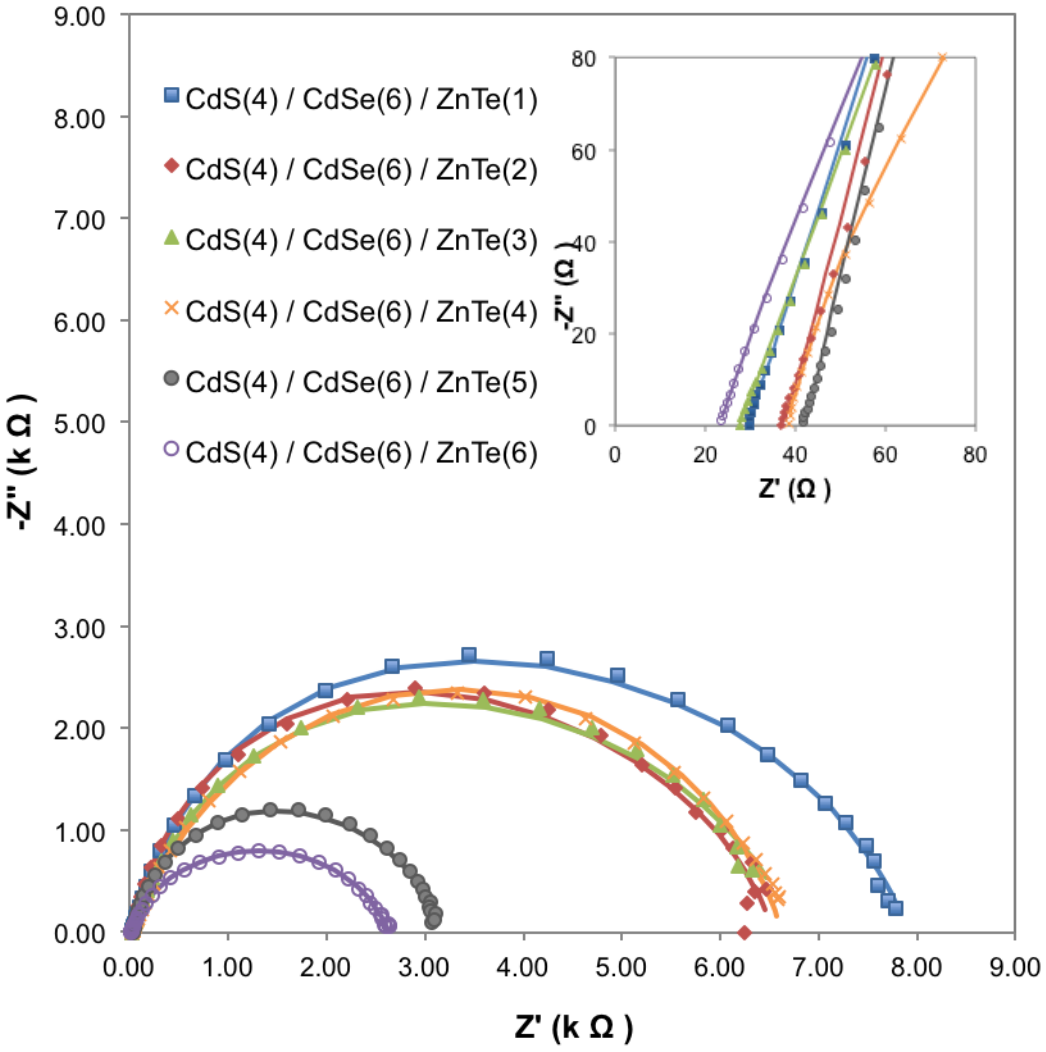

Figure 7.16. Nyquist plots of CdS(4)/CdSe(6)/ZnTe(*n*) QDSSCs under dark with 0.45 V bias. Details of the plots at high-frequencies are shown in the inset. Solid lines are the fitted curves.

Table 7.9. EIS results of CdS(4)/CdSe(6)/ZnTe(*n*) QDSSCs under dark with 0.45 V bias: series resistance, charge-transfer resistance, impedance and electron lifetime.

	R_S (Ω)	R_r (k Ω)	CPE2-T (μ S.s^n)	CPE2-P (0<n<1)	τ (m s)
CdS(4) / CdSe(6) / ZnTe(1)	29.12	2.27	7.71	0.99	16.74
CdS(4) / CdSe(6) / ZnTe(2)	37.15	2.32	5.68	1.00	13.18
CdS(4) / CdSe(6) / ZnTe(3)	27.38	1.79	8.28	0.96	12.38
CdS(4) / CdSe(6) / ZnTe(4)	37.99	3.50	8.82	0.80	12.86
CdS(4) / CdSe(6) / ZnTe(5)	42.07	2.22	12.53	0.81	11.67
CdS(4) / CdSe(6) / ZnTe(6)	22.99	0.99	20.34	0.80	7.53

7.3 Summary

Co-sensitized solar cells were prepared with CdS and CdSe QDs and optimized with respect to the number of SILAR cycles used for the QD deposition. The best performance was obtained with photoanode having CdS(4)/CdSe(6) structure. By passivating the QDs co-sensitized TiO_2 film with ZnS, an efficiency of 1.37% was obtained. However, when the ZnS layer was replaced with ZnSe or ZnTe, there was no significant improvement in the solar cell performance. Nevertheless, ZnSe has the potential to be applied as photocurrent transporter in a cascade QD structure. ZnTe, on the other hand, is not recommended for the application in QDSSC as its implication is not that significant.

7.4 References

[1] Ruhle, S., Yahav, S., Greenwald, S., & Zaban, A. (2012). Importance of recombination at the TCO/electrolyte interface for high efficiency quantum dot sensitized solar cells. *Journal of Physical Chemistry C, 116,* 17473-17478.

[2] Tachan, Z., Hod, I., Shalom, M., Grinis, L., & Zaban, A. (2013). The importance of the TiO_2/quantum dots interface in the recombination processes of quantum dot sensitized solar cells. *Physical Chemistry Chemical Physics, 15,* 3841-3845.

[3] Shen, Q., Kobayashi, J., Diguna, L.J., & Toyoda, T. (2008). Effect of ZnS coating on the photovoltaic properties of CdSe quantum dot-sensitized solar cells. *Journal of Applied Physics, 103,* 084304.

[4] Fuente, M.S.d.l., Sanchez, R.S., Gonzalez-Pedro, V., Boix, P.P., Mhaisalkar, S.G., Rincon, M.E., *et al.* (2013). Effect of organic and inorganic passivation in

quantum-dot-sensitized solar cells. *Journal of Physical Chemistry Letters, 4,* 1519-1525.

[5] Toyoda, T., Sato, J., & Shen, Q. (2003). Effect of sensitization by quantum-sized CdS on photoacoustic and photoelectrochemical current spectra of porous TiO_2 electrodes. *Review of Scientific Instruments, 74,* 297-299.

[6] Barcelo, I., Lana-Villarreal, T., & Gomez, R. (2011). Efficient sensitization of ZnO nanoporous films with CdSe grown by Successive Ionic Layer Adsorption and Reaction (SILAR). *Journal of Photochemistry and Photobiology A: Chemistry, 220,* 47-53.

[7] Wang, X., Koleilat, G.I., Tang, J., Liu, H., Kramer, I.J., Debnath, R., *et al.* (2011). Tandem colloidal quantum dot solar cells employing graded recombination layer. *Nature Photonics, 5,* 480-484.

[8] Grätzel, M. (2001). Photoelectrochemical cells. *Nature, 414,* 338-344.

[9] Bang, J.H., & Kamat, P.V. (2009). Quantum dot sensitized solar cells. A tale of two semiconductor nanocrystals: CdSe and CdTe. *ACS Nano, 3,* 1467-1476.

[10] Seo, M.-H., Hwang, W.-P., Kim, Y.-K., Lee, J.-K., & Kim, M.-R. (2011). Improvement of quantum dot-sensitized solar cells based on Cds and CdSe quantum dots. *37th IEEE Photovoltaic Specialists Conference (PVSC),* June 19-24, 002652-002655.

[11] Zhang, Y., Zhu, J., Yu, X., Wei, J., Hu, L., & Dai, S. (2012). The optical and electrochemical properties of CdS/CdSe co-sensitized TiO_2 solar cells prepared by successive ionic layer adsorption and reaction processes. *Solar Energy, 86,* 964-971.

[12] Lee, H.J., Bang, J., Park, J., Kim, S., & Park, S.-M. (2010). Multilayered semiconductor (CdS/CdSe/ZnS)-sensitized TiO_2 mesoporous solar cells: All

prepared by successive ionic layer adsorption and reaction processes. *Chemistry of Materials, 22,* 5636-5643.

[13] Tian, J., Gao, R., Zhang, Q., Zhang, S., Li, Y., Lan, J., *et al.* (2012). Enhanced performance of CdS/CdSe quantum dot cosensitized solar cells via homogeneous distribution of quantum dots in TiO_2 film. *Journal of Physical Chemistry C, 116,* 18655-18662.

[14] Li, Z.-X., Xie, Y.-L., Xu, H., Wang, T.-M., Xu, Z.-G., & Zhang, H.-L. (2011). Expanding the photoresponse range of TiO_2 nanotube arrays by CdS/CdSe/ZnS quantum dots co-modification. *Journal of Photochemistry and Photobiology A: Chemistry, 224,* 25-30.

[15] Chen, J., Wu, J., Lei, W., Song, J.L., Deng, W.Q., & Sun, X.W. (2010). Co-sensitized quantum dot solar cell based on ZnO nanowire. *Applied Surface Science, 256,* 7438-7441.

[16] Hossain, M.A., Jennings, J.R., Shen, C., Pan, J.H., Koh, Z.Y., Matthews, N., *et al.* (2012). CdSe-sensitized mesoscopic TiO_2 solar cells exhibiting >5% efficiency: redundancy of CdS buffer layer. *Journal of Materials Chemistry, 22,* 16235-16242.

[17] Fang, S.-Q., Kim, D., Kim, J.-J., Jung, D.W., Kang, S.O., & Ko, J. (2009). Highly efficient CdSe quantum-dot-sensitized TiO_2 photoelectrodes for solar cells applications. *Electrochemistry Communications, 11,* 1337-1339.

[18] Yu, X.-Y., Lei, B.-X., Kuang, D.-B., & Su, C.-Y. (2012). High performance and reduced charge recombination of CdSe/CdS quantum dot-sensitized solar cells. *Journal of Materials Chemistry, 22,* 12058-12063.

[19] Gonzalez-Pedro, V., Xu, X., Mora-Sero, I., & Bisquert, J. (2010). Modeling high-efficiency quantum dot sensitized solar cells. *ACS Nano, 4,* 5783-5790.

[20] Wang, Q., Moser, J.-E., & Grätzel, M. (2005). Electrochemical impedance spectroscopy analysis of dye-sensitized solar cells. *Journal of Physical Chemistry B, 109*, 14945-14953.

[21] Fabregat-Santiago, F., Bisquert, J., Garcia-Belmonte, G., Boschloo, G., & Hagfeldt, A. (2005). Influence of electrolyte in transport and recombination in dye-sensitized solar cells studied by impedance spectroscopy. *Solar Energy Materials and Solar Cells, 87,* 117-131.

[22] Fabregat-Santiago, F., Garcia-Belmonte, G., Bisquert, J., Zaban, A., & Salvador, P. (2002). Decoupling of transport, charge storage, and interfacial charge transfer in the nanocrystalline TiO_2/electrolyte system by impedance methods. *Journal of Physical Chemistry B, 106,* 334-339.